THE JOURNAL OF PHYSICAL CHEMISTRY A LETTERS

2009, *113,* 945–948
Published on Web 11/14/2008

Photoelectron Angular Distribution and Molecular Structure in Multiply Charged Anions

Xiao-Peng Xing, Xue-Bin Wang, and Lai-Sheng Wang*

Department of Physics, Washington State University, 2710 University Drive, Richland, Washington 99354, and Chemical & Materials Sciences Division, Pacific Northwest National Laboratory, MS K8-88, Richland, Washington 99352

Received: August 16, 2008

Photoelectrons emitted from multiply charged anions (MCAs) carry information of the intramolecular Coulomb repulsion (ICR), which is dependent on molecular structures. Using photoelectron imaging, we observed the effects of ICR on photoelectron angular distributions (PAD) of the three isomers of benzene dicarboxylate dianions $C_6H_4(CO_2)_2^{2-}$ (*o*-, *m*- and *p*-BDC^{2-}). Photoelectrons were observed to peak along the laser polarization due to the ICR, but the anisotropy was the largest for *p*-BDC^{2-}, followed by the *m*- and *o*-isomer. The observed anisotropy is related to the direction of the ICR or the detailed molecular structures, suggesting that photoelectron imaging may allow structural information to be obtained for complex multiply charged anions.

Introduction

Photoelectron spectroscopy (PES) is a powerful technique to probe the electronic structure and chemical bonding of molecules and clusters. Angle-resolved PES provides additional information about the photoionization dynamics and the nature of the bound molecular orbitals, from which electrons are emitted. Within the dipole approximation, the angular distribution of photoelectrons for nonoriented molecules with linearly polarized light is described by the Cooper−Zare formula,[1] $I(\theta) = c[1 + \beta P_2(\cos\theta)]$, where θ is the angle between the laser polarization and the velocity vector of the photoelectron, $P_2(\cos\theta)$ is the second-order Legendre polynomial, β is the anisotropy parameter, and c is a constant proportional to the total detachment cross section. The anisotropy parameter (β), which ranges from −1 for pure perpendicular transitions to +2 for pure parallel transitions, contains all the dynamical information for the photoemission event. Using photoelectron imaging, however, we have shown very recently that for multiply charged anions (MCAs) the Cooper−Zare formula is no longer appropriate because the photoelectron angular distributions are governed by the intramolecular Coulomb repulsion (ICR).[2] Here we show that photoelectron imaging can provide structural information for complex MCAs because the ICR is highly sensitive to molecular structures.

MCAs are ubiquitous in the condensed phase, but they have only become accessible for detailed spectroscopic characterization[3−6] since the invention of the electrospray ionization technique.[7] The stability of isolated MCAs is governed by the ICR due to the excess charges,[8−11] which make MCAs rather fragile and difficult to study in the gas phase.[12,13] We have developed an electrospray-PES apparatus,[14] which has allowed a wide range of MCAs to be investigated in the gas phase. The repulsive Coulomb barrier that exists universally in MCAs was directly observed by PES,[3,4] as well as metastable MCAs with negative electron binding energies.[15−18] The strong intramolecular Coulomb repulsion was expected to have major effects on the electron emission dynamics and photoelectron angular distribution (PAD) of MCAs, which was observed in a very recent study on a series of linear dicarboxylate dianions [$^-O_2C(CH_2)_nCO_2^-$, $DC(n)^{2-}$, $n = 3-10$].[2] It was shown that the PAD of these dianions was strongly affected by the ICR, which forces the photoelectrons to emit along the molecular axis parallel to the laser polarization.

Experiment

The imaging method was originally developed to record spatial distributions of photodissociation products[19] and has been extended to PES.[20] Over the past decade, photoelectron imaging has become a highly valuable technique for anions because of its high sensitivity and capability to yield angular distributions.[21−27] The present study was carried out on our electrospray PES apparatus[14] by replacing the original magnetic-bottle photoelectron analyzer with a velocity map imaging system.[28] The anions of interest were produced via electrospray of their respective salt solutions at ∼1 mM concentration in a mixed water/methanol solvent (1/3 in volume), as described previously.[29] Each anion of interest was mass selected and directed into the center of the photoelectron imaging lens system, where they were detached by a linearly polarized laser beam [355 nm (3.496 eV) or 266 nm (4.661 eV)] from a Nd:YAG laser. The laser polarization was always parallel to the imaging plane. The nascent electron cloud was accelerated by a high voltage pulse applied to the imaging electrodes and was projected onto a phosphor screen behind a set of microchannel plates. The positions of the photoelectrons on the phosphor screen were recorded by a CCD camera and accumulated as a photoelectron image. The electron kinetic energy (KE) resolution (ΔKE/KE) ranges from 3.7% for low energy electrons to 2.5% for electrons above 1 eV, as calibrated from the 355 nm spectrum of Br^- and the 266 nm spectrum of I^-.

* To whom correspondence should be addressed. E-mail: ls.wang@pnl.gov.

10.1021/jp8073442 CCC: $40.75

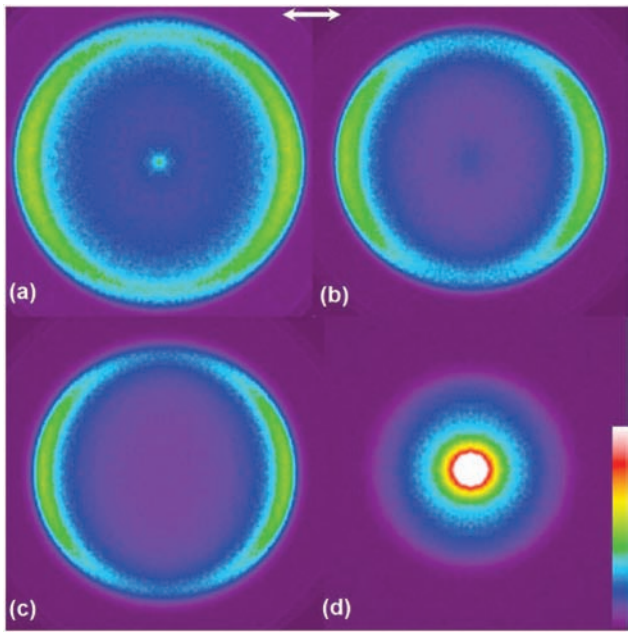

Figure 1. Photoelectron images of (a) *o*-$C_6H_4(CO_2)_2^{2-}$, (b) *m*-$C_6H_4(CO_2)_2^{2-}$, (c) *p*-$C_6H_4(CO_2)_2^{2-}$ at 355 nm (3.496 eV), and (d) $C_6H_5CO_2^-$ at 266 nm (4.661 eV). The scale bar is given on the right bottom corner. The double arrow in the top indicates the directions of the laser polarization.

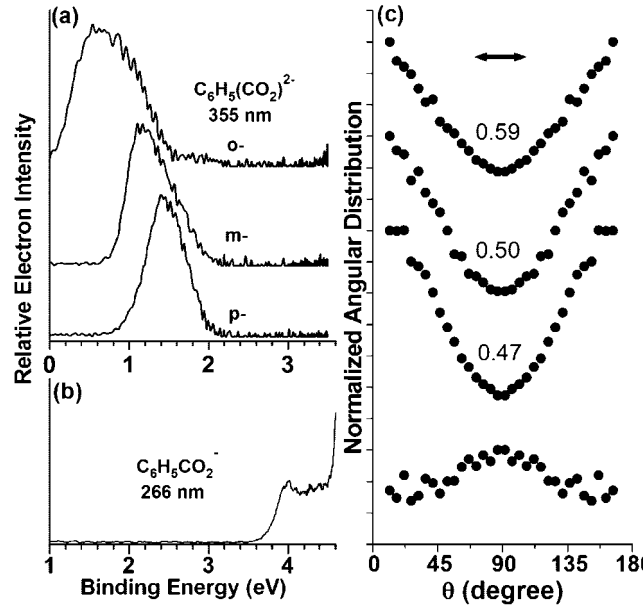

Figure 2. Photoelectron spectra of (a) *o*-, *m*-, *p*-$C_6H_4(CO_2)_2^{2-}$, and (b) $C_6H_5CO_2^-$ obtained from the images in Figure 1. Photoelectron kinetic energies (KE) were obtained from the radius (R) of the images, KE $\propto R^2$, calibrated by the photoelectron images of Br^- and I^-. The electron binding energies (BE) were determined by BE $= h\nu -$ KE. The photoelectron intensities were obtained by integrating all angles after inverse Abel transformation. (c) Photoelectron angular distributions $I(\theta)$ (integrated for signals within ~0.8 eV starting from the threshold) normalized to one for the maximum intensity in each frame. The vertical scale is 0.1 per tick. Because of symmetry, only half of the image from Figure 1 is plotted from $\theta = 0°$ to 180°. The double arrow represents the directions of the laser polarization. The numbers in (c) show the relative intensities of the minimum point for each plot.

Results

Figure 1 shows the photoelectron images of *o*-, *m*- and *p*-BDC^{2-} at 355 nm compared to that of $C_6H_5CO_2^-$ at 266 nm. The single outer ring in Figure 1a−c implies that only one detachment band is accessed at this photon energy, consistent with the previous PES study using a magnetic-bottle photoelectron analyzer.[29] Interestingly, the photoelectron signals of *o*-, *m*- and *p*-BDC^{2-} exhibit strong anisotropies, peaking along the direction of the laser polarization. The anisotropy clearly increases from the *o*- → *m*- → *p*-isomer. Figure 1d displays the photoelectron image of the singly charged monocarboxylate $C_6H_5CO_2^-$ at 266 nm as a control experiment. Several fairly isotropic rings were revealed with a strong threshold band (the central spot). Figure 2a,b displays the PES spectra in binding energies obtained from the images in Figure 1 after inverse Abel transformations and integrations of electron signals at all angles.[30] The spectra of the three dianions look identical to those measured previously using the magnetic-bottle apparatus.[29] The electron binding energy increases from the *o*- to *m*- to *p*-isomer, reflecting the different magnitudes of the ICR in the three isomers (*o*- > *m*- > *p*-isomer). The spectral cutoff in the high binding energy range in Figure 2a was due to the repulsive Coulomb barrier that exists universally in MCAs.[3−5] The strong threshold feature for $C_6H_5CO_2^-$ was shown also very clearly in Figure 2b, which was likely due to a resonant enhancement because the 266 nm photon occurs right at the second detachment band.[31]

Figure 2c shows the PAD by integrating the main body of the first photodetachment band in each case after inverse Abel transformation of the photoelectron images in Figure 1. The maximum intensity for each plot is normalized to one. The PAD plots are essentially numerical representations of the anisotropies revealed by the images in Figure 1. Because of symmetry, only half of the ring from 0° to 180° (defined to be along the laser polarization direction) is plotted in each case. The maxima along the laser polarization at $\theta = 0°$ and 180° and the minimum perpendicular to the laser polarization at $\theta = 90°$ are clearly shown in all three dianions. However, the opposite was observed for $C_6H_5CO_2^-$, which was shown to be a perpendicular transition with maximum intensity at $\theta = 90°$.[32] The relative magnitude of the minimum for the three dianions is given in Figure 2c, consistent with the increasing anisotropy in the direction of *p*- > *m*- > *o*-BDC^{2-}.

Discussion

As shown in our recent work,[2] the PAD for MCAs is strongly influenced by the ICR, which directs the photoelectrons along the direction of the ICR, regardless of the initial electron emission directions. Photodetachment of the linear dicarboxylates, $DC(n)^{2-}$, involves a perpendicular transition from the terminal carboxylate groups if the dianions are aligned with the laser polarization. However, the ICR forces electrons to be emitted along the aliphatic chain, yielding an effective parallel transition for shorter chains due to the strong ICR. A gradual change from parallel to perpendicular transitions was observed as the chain length increases (i.e., as the ICR decreases).[2] The chromophore ($-CO_2^-$) for photodetachment in both the benzene carboxylates and the previous aliphatic carboxylates is the same, as also proven by the perpendicular transition observed for the benzene monocarboxylate. The first PES band involves photodetachment from two oxygen lone-pair molecular orbitals, b_2 and a_1 under the local C_{2v} symmetry of the $-CO_2^-$ group.[31] But the cross section for photodetachment from the a_1 orbital is relatively low and the first detachment band primarily contains contributions from the b_2 orbital, which is similar to the b_2 orbital in the C_{2v} CS_2^-. The latter was previously observed to yield a perpendicular transition,[33] which was interpreted using symmetry

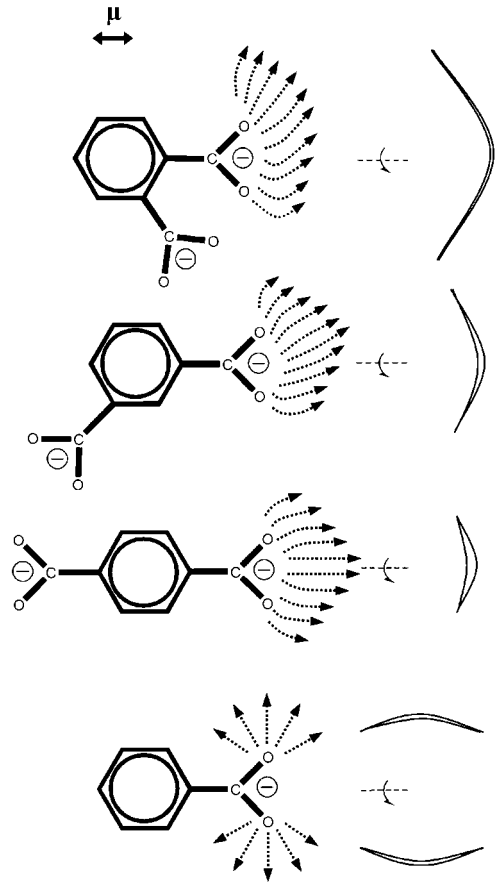

Figure 3. Schematics illustrating how the photoelectron trajectories are influenced by the intramolecular Coulomb repulsion for *o*-, *m*-, *p*-$C_6H_4(CO_2)_2^{2-}$. The perpendicular transition for $C_6H_5CO_2^-$ is shown in the bottom for comparison. The laser polarization is shown at the top with the double arrows. The lobes on the right-hand side schematically illustrate the photoelectron distributions and the effects of rotation around the laser polarization.

arguments and the so-called "s-p" model by neglecting the outgoing partial electron waves with $l > 1$. The similarity between $-CO_2^-$ and CS_2^- also implies that the detachment cross section is the largest for $-CO_2^-$ when its C_2 axis is aligned with the laser polarization. Therefore, the observed parallel transitions for the three BDC^{2-} isomers are clearly due to the ICR.

A question arises, why does the anisotropy for *o*-BDC^{2-} appear to be the weakest whereas its ICR is the strongest? Clearly, the molecular structure here plays a key role in determining the details of the PAD for MCAs. The different PADs and anisotropies observed for the three BDC^{2-} isomers can be understood using the schematics shown in Figure 3. The schematic for the benzene monocarboxylate shows the nature of the perpendicular electron emission when the carboxylate group is aligned with the laser polarization. In the case of *p*-BDC^{2-}, the two carboxylate groups are aligned on the same molecular axis. Thus, electrons emitted from one of the carboxylates would feel the strong Coulomb repulsion from the remaining charged group, giving rise to the maximum electron intensities along the laser polarization direction, despite the fact that this is a perpendicular transition.

However, when one of the carboxylates is aligned with the laser polarization for the *m*- or *o*-isomer, the other carboxylate is off axis, as shown in Figure 3. Thus, the direction of the ICR and the electron trajectories will also be off axis relative to the laser polarization, as schematically illustrated in Figure 3. Moreover, in the case of *p*-BDC^{2-}, the molecular rotation around the laser polarization would have no effects on the PAD, but molecular rotation by the *m*- and *o*-isomer around the laser polarization would have profound effects on the PAD because the other charge is off axis. The rotation would essentially spread out the PAD and give rise to the apparent reduced anisotropy. Because the second carboxylate group of *o*-BDC^{2-} is more severely off axis and it possesses the strongest ICR, it is easy to understand that this isomer would yield the largest spread in the PAD, as observed experimentally.

Thus, using photoelectron imaging, we have observed influences of molecular structures on photoelectron angular distributions of MCAs with localized charge carriers. The effects originate from the strong intramolecular Coulomb repulsion present in MCAs. These effects may be used to obtain structural information for complex MCAs by photoelectron imaging. In the current cases, only qualitative structural information can be glimpsed because the MCAs are not oriented. It is conceivable that more direct and quantitative structural information may be obtained with oriented MCAs.

Acknowledgment. We thank Prof. M. A. Johnson and his group for valuable discussions and help during the construction of the imaging analyzer and Prof. H. Reisler for the BASEX program used for the inverse Abel transform. This work was supported by the U.S. Department of Energy, Office of Basic Energy Sciences, Chemical Science Division and partly by NSF and performed at the W. R. Wiley Environmental Molecular Sciences Laboratory, a national scientific user facility sponsored by DOE's Office of Biological and Environmental Research and located at Pacific Northwest National Laboratory, which is operated for DOE by Battelle.

References and Notes

(1) Cooper, J.; Zare, R. N. *J. Chem. Phys.* **1968**, *48*, 942.
(2) Xing, X. P.; Wang, X. B.; Wang, L. S. *Phys. Rev. Lett.* **2008**, *101*, 083008.
(3) Wang, X. B.; Ding, C. F.; Wang, L. S. *Phys. Rev. Lett.* **1998**, *81*, 3351.
(4) Wang, L. S.; Ding, C. F.; Wang, X. B.; Nicholas, J. B. *Phys. Rev. Lett.* **1998**, *81*, 2667.
(5) Wang, L. S.; Wang, X. B. *J. Phys. Chem. A* **2000**, *104*, 1978.
(6) Friedrich, J.; Gilb, S.; Ehrler, O. T.; Behrendt, A.; Kappes, M. M. *J. Chem. Phys.* **2002**, *117*, 2635.
(7) Fenn, J. B. *Angew. Chem., Int. Ed.* **2003**, *42*, 3871.
(8) Schauer, S. N.; Williams, P.; Compton, R. N. *Phys. Rev. Lett.* **1990**, *65*, 625.
(9) Scheller, M. K.; Compton, R. N.; Cederbaum, L. S. *Science* **1995**, *270*, 1160.
(10) Boldyrev, A. I.; Gutowski, M.; Simons, J. *Acc. Chem. Res.* **1996**, *29*, 497.
(11) Dreuw, A.; Cederbaum, L. S. *Chem. Rev.* **2000**, *102*, 181.
(12) Kalcher, J.; Sax, A. F. *Chem. Rev.* **1994**, *94*, 2291.
(13) Freeman, G. R.; March, N. H. *J. Phys. Chem.* **1996**, *100*, 4331.
(14) Wang, L. S.; Ding, C. F.; Wang, X. B.; Barlow, S. E. *Rev. Sci. Instrum.* **1999**, *70*, 1957.
(15) Wang, X. B.; Wang, L. S. *Nature* **1999**, *400*, 245.
(16) Wang, X. B.; Ferris, K.; Wang, L. S. *J. Phys. Chem. A* **2000**, *104*, 25.
(17) Weis, P.; Hampe, O.; Gilb, S.; Kappes, M. M. *Chem. Phys. Lett.* **2000**, *321*, 426.
(18) Yang, J.; Xing, X. P.; Wang, X. B.; Wang, L. S.; Sergeeva, A. P.; Boldyrev, A. I. *J. Chem. Phys.* **2008**, *128*, 091102.
(19) Chandler, D. W.; Houston, P. L. *J. Chem. Phys.* **1987**, *87*, 1445.
(20) Helm, H.; Bjerre, N.; Dyer, D. J.; Huestis, D. L.; Saeed, M. *Phys. Rev. Lett.* **1993**, *70*, 3221.
(21) Pinare, J. C.; Baguenard, B.; Bordas, C.; Broyer, M. *Phys. Rev. Lett.* **1998**, *81*, 2225.
(22) Deyerl, H. J.; Alconcel, L. S.; Continetti, R. E. *J. Phys. Chem. A* **2001**, *105*, 552.
(23) Surber, E.; Sanov, A. *J. Chem. Phys.* **2002**, *116*, 5921.
(24) Davis, A. V.; Wester, R.; Bragg, A. E.; Neumark, D. M. *J. Chem. Phys.* **2003**, *118*, 999.

(25) Rathbone, G. J.; Sanford, T.; rews, D.; Lineberger, W. C. *Chem. Phys. Lett.* **2005**, *401*, 570.

(26) Sobhy, M. A.; Castleman, A. W. *J. Chem. Phys.* **2007**, *126*, 154314.

(27) McCunn, L. R.; Gardenier, G. H.; Guasco, T. L.; Elliott, B. M.; Bopp, J. C.; Relph, R. A.; Johnson, M. A. *J. Chem. Phys.* **2008**, *128*, 234311.

(28) Eppink, A. T. J. B.; Parker, D. H. *Rev. Sci. Instrum.* **1997**, *68*, 3477.

(29) Wang, X. B.; Nicholas, J. B.; Wang, L. S. *J. Chem. Phys.* **2000**, *113*, 653.

(30) Dribinski, V.; Ossadtchi, A.; Mandelshtam, V. A.; Reisler, H. *Rev. Sci. Instrum.* **2002**, *73*, 2634.

(31) Woo, H. K.; Wang, X. B.; Kiran, B.; Wang, L. S. *J. Phys. Chem. A* **2005**, *109*, 11395.

(32) The anisotropy observed for the benzene monocarboxylate was unusually weak, which might be due to the fact that the detachment band was close to the threshold at 266 nm.

(33) Surber, E.; Mabbs, R.; Sanov, A. *J. Phys. Chem. A* **2003**, *107*, 8215.

JP8073442